Possible bicollinear nematic state with monoclinic lattice distortions in iron telluride compounds

Christopher B. Bishop, Jacek Herbrych, Elbio Dagotto, and Adriana Moreo
Department of Physics and Astronomy, University of Tennessee, Knoxville, Tennessee 37966, USA
and Materials Science and Technology Division, Oak Ridge National Laboratory, Oak Ridge, Tennessee 37831, USA
(Received 6 April 2017; revised manuscript received 11 July 2017; published 24 July 2017)

Iron telluride (FeTe) is known to display bicollinear magnetic order at low temperatures together with a monoclinic lattice distortion. Because the bicollinear order can involve two different wave vectors $(\pi/2,\pi/2)$ and $(\pi/2,-\pi/2)$, symmetry considerations allow for the possible stabilization of a nematic state with short-range bicollinear order coupled to monoclinic lattice distortions at a T_S higher than the temperature T_N where long-range bicollinear order fully develops. As a concrete example, the three-orbital spin-fermion model for iron telluride is studied with an additional coupling $\tilde{\lambda}_{12}$ between the monoclinic lattice strain and an orbital-nematic order parameter with B_{2g} symmetry. Monte Carlo simulations show that with increasing $\tilde{\lambda}_{12}$ the first-order transition characteristic of FeTe splits and bicollinear nematicity is stabilized in a (narrow) temperature range. In this new regime, the lattice is monoclinically distorted and short-range spin and orbital order breaks rotational invariance. A discussion of possible realizations of this exotic state is provided.

DOI: 10.1103/PhysRevB.96.035144

I. INTRODUCTION

The theoretical understanding of high critical temperature superconductivity in iron compounds has evolved from its early qualitative developments based on Fermi surface nesting to more quantitative efforts incorporating the role of electronic correlations [1–6]. In particular, experts have focused on several complex regimes including electronic nematicity [7–10], an interesting state observed in several high critical temperature pnictide superconductors [11–14]. Upon cooling, this nematic phase is reached at a temperature T_S, concomitantly with a structural phase transition from a tetragonal to an orthorhombic lattice. Upon further cooling, a magnetically ordered phase is stabilized at a lower temperature T_N. The orthorhombic nematic phase between T_S and T_N exhibits a reduced symmetry under rotations from C_4 to C_2. This is also observed in the magnetic and orbital degrees of freedom leading to nonzero magnetic and orbital "nematic" order parameters. Experimental investigations have shown that this nematic phase occurs in the parent compounds of the 1111 pnictides [11]. Since the orthorhombic lattice distortion $\delta_O = |a_O - b_O|/(a_O + b_O) \sim 0.004$ [15] is small (a_O and b_O are the lattice parameters in the orthorhombic notation), it is often argued that the lattice plays the role of a "passenger" in the nematic transition which is believed to be driven by either the magnetic or orbital degrees of freedom. In addition, it is interesting to notice that the structural transition occurs simultaneously with the Néel temperature in several other iron-based materials. For example, members of the 122 family need to be electron doped, with the chemical replacement occurring directly on the FeAs planes, to develop the nematic phase [12–14]. Hole doping, or electron doping via chemical substitution away from the FeAs planes, fails to establish nematicity [16,17].

In the chalcogenides, the parent compound FeTe exhibits an unexpected "bicollinear" magnetic state [18–20], shown in panels (a) and (b) of Fig. 1, whose T_N coincides with the T_S of a structural transition to a phase with a monoclinic lattice distortion, as shown in panel (d) of the same figure. This joint transition is strongly first order [18,21,22]. The reported lattice distortions in $Fe_{1.076}Te$ and $Fe_{1.068}Te$ are $\delta_M = |a_M - b_M|/(a_M + b_M) \sim 0.007$ [18] (a_M and b_M are the low-temperature lattice parameters in the monoclinic notation). Replacing Te with Se, the bicollinear magnetic order is eventually lost, the material becomes superconducting, and it develops an orthorhombic nematic phase above its superconducting critical temperature. In recent theoretical work, using a spin-fermion model, we explained the bicollinear magnetic order using symmetry considerations as a consequence of the monoclinic distortion [23,24]. Based on this reasoning, the role of the lattice in the case of FeTe appears more important than previously anticipated.

The aim of the present work is to argue that the pnictides and chalcogenides could potentially behave more symmetrically with regards to the presence of a nematic state. As expressed above, the pnictides either already have nematicity without doping, as in the 1111 compounds, or develop nematicity after doping as in the Co-doped 122 compounds. Based on symmetry arguments, the presence of a nematic regime is theoretically understood as follows. In these materials, the magnetic ground state has wave vector $(\pi,0)$, with staggered spins along the x axis and parallel spins along the y axis. However, the $(0,\pi)$ state should have the same energy by symmetry. In cases of twofold degeneracy in the ground state, it was predicted that an Ising transition could occur upon cooling [25], with an order parameter that breaks lattice rotational invariance and involves only short-range magnetic correlations. Upon further cooling, the O(3) full symmetry breaking process is possible.

Our main observation here is that the bicollinear state shown in Fig. 1(a) with wave vector $\mathbf{k_1} = (\pi/2, -\pi/2)$ has a partner, displayed in Fig. 1(b), with identical energy but $\mathbf{k_2} = (\pi/2,\pi/2)$ [26]. Then, the same Ising-O(3) rationale expressed above for the $(\pi,0) - (0,\pi)$ degeneracy can be repeated for bicollinear states: starting at high temperature, both spin structure factors $S(\mathbf{k})$ will start growing with equal strength upon cooling at the wave vectors $\mathbf{k_1}$ and $\mathbf{k_2}$. By analogy with the pnictides, it is possible that at a critical nematic temperature T_S, an asymmetry develops such that

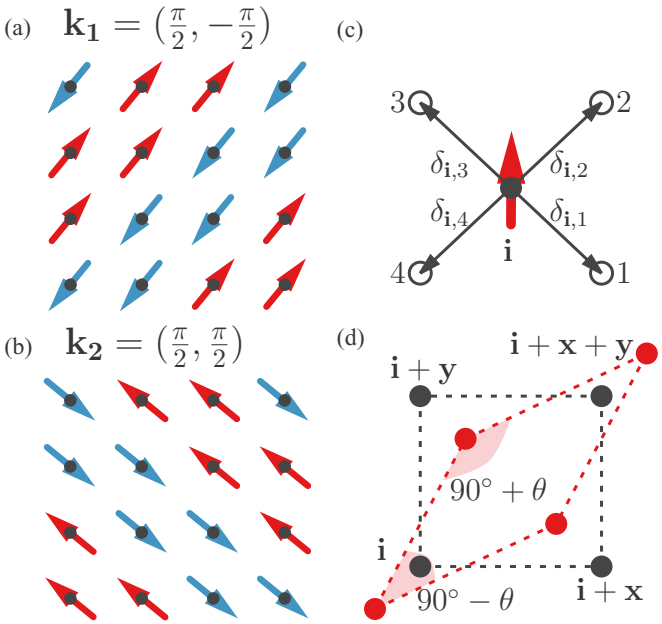

FIG. 1. (a) The bicollinear antiferromagnetic spin order with wave vector $(\pi/2, -\pi/2)$. (b) Same as (a) but for the state lattice rotated by 90 degrees with wave vector $(\pi/2,\pi/2)$. (c) Schematic drawing of an iron atom at site $\mathbf{i}$ (filled symbol) and its four Te neighbors (open symbols), projected in the $x-y$ plane in their equilibrium position. The distances $\delta_{\mathbf{i},\nu}$ between the irons at site $\mathbf{i}$ and its four neighboring Te atoms are indicated as well. The localized spin $\mathbf{S_i}$ is also sketched. (d) Schematic drawing of the Fe lattice equilibrium position in the tetragonal phase (black symbols and lines) and in the monoclinic phase (red symbols and lines). Four Fe atoms are indicated with filled symbols and labeled by their lattice site index.

$S(\mathbf{k_1}) > S(\mathbf{k_2})$, and then at a lower temperature T_N, $S(\mathbf{k_2})$ drops to zero while $S(\mathbf{k_1})$ grows like the volume.

While no nematic phase with these characteristics has been reported yet in materials of the FeTe family with the bicollinear spin order, the present study provides computational evidence that there are Hamiltonians with spin- and orbital-lattice coupling that display this new nematic behavior if the coupling strengths are properly tuned. While our many-body tools do not allow us to predict what specific material may display this phenomenon, our symmetry arguments and concrete simulation results are offered as motivation for the experimental search for this exotic bicollinear-nematic state.

Previous numerical studies of spin-fermion models for pnictides with spin, orbital, and lattice degrees of freedom provided indications that the structural transition is due to the coupling between the lattice and spins [27]. Thus, in these regards, the lattice follows the spins. But the spin-lattice coupling leads to $T_S = T_N$ and, then, the establishment of a nematic phase with $T_S > T_N$ requires a more subtle mechanism. Investigations by our group have shown that the nematic regime can be achieved by the addition of an orbital-lattice coupling [27] (or by the introduction of in-plane magnetic disorder, namely by replacing iron by nonmagnetic atoms [28,29]). Based on this previous research, here a coupling between the monoclinic lattice distortion and an *orbital* nematic parameter with B_{2g} symmetry will be added to the spin-fermion model that already has the spin-lattice coupling previously developed to study FeTe [23]. It will be shown below that this addition generates the novel bicollinear nematic state. This is not an obvious result because the tight-binding term contains an intrinsic tendency towards collinear magnetic order that could have affected the fragile nematicity region that we are reporting here.

The publication is organized as follows. In Sec. II, the model is described including the new term that must be incorporated in order to stabilize a bicollinear-nematic state. In Sec. III, we provide an explanation of the numerical approach that allows for the parallelization of the Monte Carlo procedure and the concomitant use of clusters of reasonable size for our purposes. The main results showing the stabilization of the new nematic state are presented in Sec. IV. The discussion, including possible physical realizations, is in Sec. V, with brief conclusions in Sec. VI.

II. MODELS

In the first section, we will discuss a general model that addresses the interactions between electrons and the lattice for the case of monoclinic distortions. In the second section, the actual special case that was computationally investigated in this publication will be presented. Our effort aims to prove that there is at least one set of couplings for which, varying temperature, a bicollinear nematic state is stabilized. A more comprehensive analysis of phase diagrams varying the many couplings in the generic model would demand considerable computational resources and this task is left for future investigations.

A. Generic model

The most general spin-fermion (SF) Hamiltonian discussed here is an extension of the purely electronic model previously introduced [30,31], supplemented by additional couplings to the monoclinic lattice degrees of freedom [27,32,33]:

$$H_{\mathrm{SF}} = H_{\mathrm{Hopp}} + H_{\mathrm{Hund}} + H_{\mathrm{Heis}} + H_{\mathrm{Stiff}} + H_{\mathrm{SLM}} + H_{\mathrm{OLM}}. \tag{1}$$

H_{Hopp} represents the three-orbitals (d_{xz}, d_{yz}, d_{xy}) tight-binding Fe-Fe hopping of electrons, with the hopping amplitudes selected to reproduce photoemission data (see Eqs. (1)–(3) and Table 1 of Ref. [34]). In the undoped limit, the average electronic density per iron and per orbital is set to $n = 4/3$ [34] and a chemical potential in H_{Hopp} [33] controls its value. The on-site Hund interaction is $H_{\mathrm{Hund}} = -J_{\mathrm{H}} \sum_{\mathbf{i},\alpha} \mathbf{S_i} \cdot \mathbf{s}_{\mathbf{i},\alpha}$, where $\mathbf{S_i}$ are the localized spins at site $\mathbf{i}$ and $\mathbf{s}_{\mathbf{i},\alpha}$ are spins corresponding to orbital α of the itinerant fermions at the same site. For computational simplicity, the localized spins are assumed classical and of norm one [35]. H_{Heis} contains the nearest neighbor (NN) and next-NN (NNN) Heisenberg interactions among the localized spins, with respective couplings J_{NN} and J_{NNN}. As explained before [27,31], both NN and NNN could be active because of the geometry of the problem, where in each layer the Te atoms (or As, Se, P) are at the centers of iron plaquettes as seen from above. However, in our previous study of FeTe [23], we observed that the experimental value of T_N for FeTe could be obtained by simply setting $J_{\mathrm{NN}} = J_{\mathrm{NNN}} = 0$.

This is due to the fact that the intersite spin-spin couplings favor either checkerboard ($J_{\rm NN}$) or collinear ($J_{\rm NNN}$) magnetic configurations and in order to obtain a bicollinear ground state it is necessary to use a larger value of the spin-lattice coupling $\tilde{g}_{12}$, which, in turn, increases T_N [36]. $H_{\rm Stiff}$ is the lattice stiffness given by a Lennard-Jones potential to speed up convergence [33] (full expression can be found in [27]).

Recently, an important novel term was introduced [23] to describe FeTe properly. This term has the form $H_{\rm SLM} = -g_{12}\sum_{\mathbf{i}}\Psi_{NNN}(\mathbf{i})\epsilon_{12}(\mathbf{i})$ and it provides a coupling between the localized spins and the monoclinic $\mathcal{M}_{\rm ono}$ lattice distortions [37]. The coupling constant strength is g_{12} and the spin NNN nematic order parameter is defined as

$$\Psi_{NNN}(\mathbf{i}) = \tfrac{1}{2}\mathbf{S}_{\mathbf{i}}\cdot(\mathbf{S}_{\mathbf{i}+\mathbf{x}+\mathbf{y}} + \mathbf{S}_{\mathbf{i}-\mathbf{x}-\mathbf{y}} - \mathbf{S}_{\mathbf{i}+\mathbf{x}-\mathbf{y}} - \mathbf{S}_{\mathbf{i}-\mathbf{x}+\mathbf{y}}), \quad (2)$$

where $\mathbf{i}\pm\mu\pm\nu$ indicates the four NNN sites to $\mathbf{i}$, with $\mu = \pm\mathbf{x}$ and $\nu = \pm\mathbf{y}$ representing unit vectors along the x and y axes, respectively. Note that $\Psi_{NNN}(\mathbf{i})$ has the value $2\,(-2)$ in the perfect bicollinear states shown in Figs. 1(a) and 1(b), respectively characterized by a peak at wave vectors $(\pi/2, -\pi/2)$ and $(\pi/2,\pi/2)$ in the magnetic structure factor. $\epsilon_{12}(\mathbf{i})$ is the lattice $\mathcal{M}_{\rm ono}$ strain defined in terms of the Fe-Te distances $\delta_{\mathbf{i},\nu}$ as

$$\epsilon_{12}(\mathbf{i}) = \tfrac{1}{8}(|\delta_{\mathbf{i},2}| + |\delta_{\mathbf{i},4}| - |\delta_{\mathbf{i},1}| - |\delta_{\mathbf{i},3}|), \quad (3)$$

where $\delta_{\mathbf{i},\nu} = (\delta^x_{\mathbf{i},\nu},\delta^y_{\mathbf{i},\nu})$ ($\nu = 1,\ldots,4$) is the distance between Fe at site $\mathbf{i}$ and each of its four Te neighbors (see panel (c) of Fig. 1 and also Fig. S1, Supplemental Material of Ref. [23]). As in previous simulations, the Te atoms are allowed to move locally from their equilibrium position only along the x and y directions because the z component of the position does not couple to the monoclinic distortion. It is important to notice that both $\Psi_{NNN}(\mathbf{i})$ and $\epsilon_{12}(\mathbf{i})$ transform according to the B_{2g} representation of the $D_{4\rm h}$ symmetry group, which means that the spin-lattice term of the Hamiltonian transforms as A_{1g} as expected. As the spin-lattice coupling g_{12} grows and induces a monoclinic $\mathcal{M}_{\rm ono}$ distortion, Ψ_{NNN} develops a nonzero expectation value leading to the bicollinear spin state order as explained in [23].

The Hamiltonian described thus far [23] leads to a first-order phase transition where both the monoclinic lattice and the bicollinear spin orders develop simultaneously. Thus no bicollinear-nematic state was reported in Ref. [23]. Based on previous investigations of pnictides using the spin-fermion model [27], it is natural to introduce a coupling between the lattice and the *orbital* degree of freedom to favor nematicity (note that adding this term does not imply immediately that the bicollinear nematic state will be stabilized because there are competing collinear tendencies in the tight-binding term; a specific calculation is thus needed, as presented below). For the new term, care with regards to the symmetry of the operators used is required. The monoclinic orbital-nematic order parameter is defined as

$$\Phi_{B_{2g}}(\mathbf{i}) = n_{\mathbf{i},XZ} - n_{\mathbf{i},YZ} = \sum_{\sigma}(c^{\dagger}_{\mathbf{i},xz,\sigma}c_{\mathbf{i},yz,\sigma} - c^{\dagger}_{\mathbf{i},yz,\sigma}c_{\mathbf{i},xz,\sigma}), \quad (4)$$

where $n_{\mathbf{i},\beta} = \sum_{\sigma} c^{\dagger}_{\mathbf{i},\beta,\sigma}c_{\mathbf{i},\beta,\sigma}$ ($\beta = XZ,YZ$), and the B_{2g} orbital basis is related to the B_{1g} orbital basis by

$$c_{\mathbf{i},XZ,\sigma} = \frac{1}{\sqrt{2}}(c_{\mathbf{i},xz,\sigma} + c_{\mathbf{i},yz,\sigma}) \quad (5)$$

and

$$c_{\mathbf{i},YZ,\sigma} = \frac{1}{\sqrt{2}}(c_{\mathbf{i},xz,\sigma} - c_{\mathbf{i},yz,\sigma}). \quad (6)$$

Notice that the x and y axes point along nearest-neighbor irons, i.e., along the sides of the plaquette formed by four irons, while the X,Y axes point along next nearest-neighbor iron, i.e., along the diagonals of the iron plaquette. The Z and z axis coincide and they are perpendicular to the plane formed by the iron layer.

The new term in the Hamiltonian $H_{\rm OLM}$ that couples the B_{2g} orbital and lattice order parameters is given by

$$H_{\rm OLM} = -\lambda_{12}\sum_{\mathbf{i}}\Phi_{B_{2g}}(\mathbf{i})\epsilon_{12}(\mathbf{i}). \quad (7)$$

Because the monoclinic lattice distortion $\epsilon_{12}(\mathbf{i})$ transforms as the B_{2g} representation of $D_{4\rm h}$, it must be coupled to an orbital order parameter that also transforms as B_{2g}, which is why $\Phi_{B_{2g}}(\mathbf{i})$ was constructed. This ensures that $H_{\rm OLM}$ is invariant under the $D_{4\rm h}$ symmetry group.

B. Parameter space studied

Although the model described thus far is generic for the spin-fermion family of Hamiltonians, including Heisenberg couplings as well as lattice-spin and lattice-orbital terms, in practice we have setup to zero some of those couplings for simplicity. The reason is that we aim to prove computationally the existence of the novel proposed bicollinear nematic state at least in the most optimal region of parameter space. In practice, it would be impossible to establish the full phase diagram varying every single parameter in the complete model, but as experiments searching for the novel phase progress, we can refine our analysis in future efforts.

$H_{\rm SF}$ was studied here with the same Monte Carlo (MC) procedure employed in Ref. [27], supplemented with the recently developed "parallel travelling cluster approximation (PTCA)" [38] described in the next section. The particular values for the couplings $J_{\rm H} = 0.1$ eV, $J_{\rm NN} = J_{\rm NNN} = 0$, and $\tilde{g}_{12} = \frac{2g_{12}}{\sqrt{kW}} = 0.24$ were chosen because they provide $T_N = T_S = 70$ K for $\lambda_{12} = 0$ [23], which is the transition temperature experimentally observed in FeTe (note then that the Heisenberg couplings are neglected in this first exploratory study, for simplicity). The coupling strength $\tilde{g}_{12}$ is the dimensionless version of the spin-lattice coupling, employing $W = 3$ eV as the bandwidth of the tight-binding term and k as the constant that appears in $H_{\rm Stiff}$ [27]. Since these couplings were discussed extensively before, in the present effort, we will instead focus on a careful description of the new dimensionless monoclinic orbital-lattice coupling $\tilde{\lambda}_{12} = \frac{2\lambda_{12}}{\sqrt{kW}}$ and its effects.

During the simulation, the Te atoms are allowed to move locally away from their equilibrium positions within the $x-y$ plane. The Fe atoms can move globally via a monoclinic distortion $\mathcal{M}_{\rm ono}$ where the angle between two orthogonal

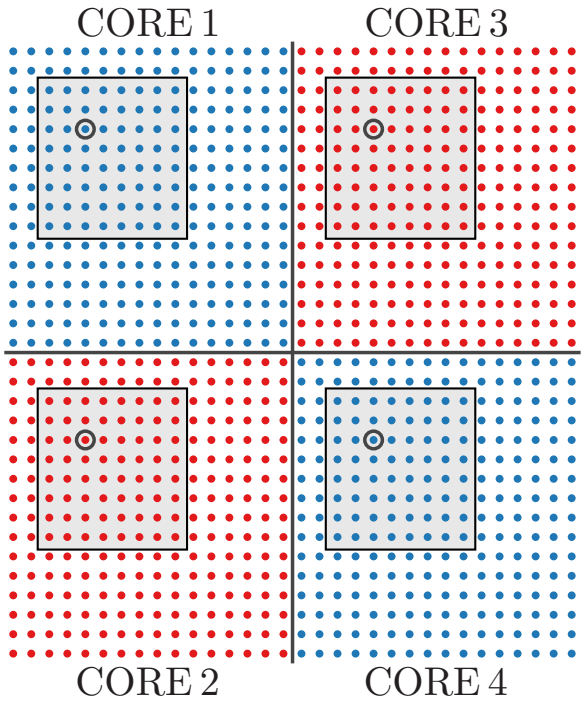

FIG. 2. Diagram of the PTCA setup used to sample the local spin and lattice variables. The lattice is divided into four quadrants and each of four processors generates traveling clusters (indicated with 8×8 squares) and proposes updates for the sites (indicated by small open circles) inside one quadrant.

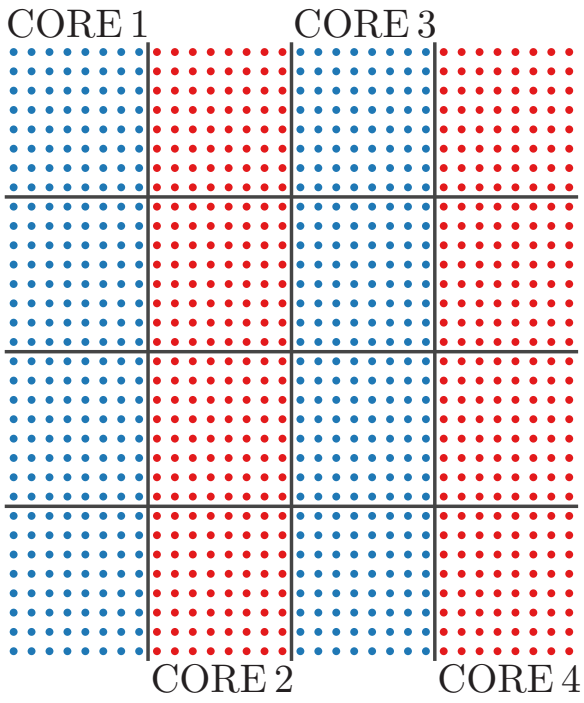

FIG. 3. Diagram of the PTCA setup used to sample the global lattice distortion variables. The lattice is divided into sixteen clusters. Each of the four processors diagonalizes four of the clusters.

Fe-Fe bonds is allowed to change globally to $90^\circ + \theta$ with the four angles in the iron plaquette adding to 360°, so that the next angle in the plaquette becomes $90^\circ - \theta$, with θ as a small angle [see Fig. 1(d)]. In addition, the localized spins $\mathbf{S_i}$ and atomic displacements $(\delta^x_{\mathbf{i},\nu},\delta^y_{\mathbf{i},\nu})$ that determine the value of the local $\mathcal{M}_{\text{ono}}$ lattice distortion $\epsilon_{12}(\mathbf{i})$ [23] [see Fig. 1(c)] are evaluated via a standard Monte Carlo procedure.

III. METHODS: THE PARALLEL TRAVELING CLUSTER APPROXIMATION

To access the lattice sizes needed to study, the existence of a monoclinic nematic phase we implemented the parallel traveling cluster approximation (PTCA) [38], which is a parallelization improvement over the traveling cluster approximation (TCA) previously introduced [39]. PTCA allows parallelization in order to use multiple CPU cores and by this procedure we can reach lattices as large as 32×32. To perform a Monte Carlo update of one of the local variables—either the localized spin $\mathbf{S_i}$ at the iron site $\mathbf{i}$ or the local distortion of the Fe-Te bonds joining the Fe atom at site $\mathbf{i}$ with its four Te neighbors—an 8×8 traveling cluster is constructed around site $\mathbf{i}$ and the Hamiltonian is diagonalized only inside that cluster to decide whether the update is accepted. The algorithm is parallelized by dividing the lattice into four quadrants with 16×16 sites, one per different CPU core. Then, each CPU generates traveling 8×8 clusters around the sites belonging to its quadrant, see Fig. 2 for an illustration, and these clusters are then simultaneously diagonalized.

To update the global monoclinic lattice distortion given by the angles in the rhombus formed by the four irons shown in Fig. 1(d) an extra new modification in the PTCA was introduced. The 32×32 sites lattice was divided into 16 clusters with 8×8 sites each as shown in Fig. 3. Each of four CPU cores was devoted to diagonalize four of the clusters as indicated in the figure. The same update is proposed in all the clusters, which are simultaneously diagonalized. Then, all the eigenvalues are collected in one of the cores in order to calculate the probability of the Monte Carlo update and decide whether the update is accepted or rejected.

For thermalization typically 5 000 Monte Carlo steps were used, while 10 000 to 25 000 steps were performed in between measurements for each set of parameters and temperatures. The spin-spin correlation functions in real space were measured and the magnetic structure factor $S(k_x,k_y)$ was calculated via their Fourier transform. Notice that in the bicollinear state the magnetic structure factor diverges for $(k_x,k_y) = (\pi/2,\pi/2)$ or $(\pi/2, -\pi/2)$. The Néel temperature T_N is obtained from the magnetic susceptibility given by

$$\chi_{S(k_x,k_y)} = N\beta\langle S(k_x,k_y) - \langle S(k_x,k_y)\rangle\rangle^2, \tag{8}$$

where $\beta = 1/k_B T$ and N is the number of lattice sites. We also calculated the numerical derivative of $S(\pi/2,\pi/2)$ with respect to temperature to double-check the value of T_N. The monoclinic structural transition temperature, T_S, was obtained by calculating the structural susceptibility given by

$$\chi_{\delta_M} = N\beta\langle\delta_M - \langle\delta_M\rangle\rangle^2, \tag{9}$$

where $\delta_M \approx \theta/2$ and θ is the deviation from 90° of the angle of the lattice plaquette as shown in Fig. 1(d) [23]. T_S was also

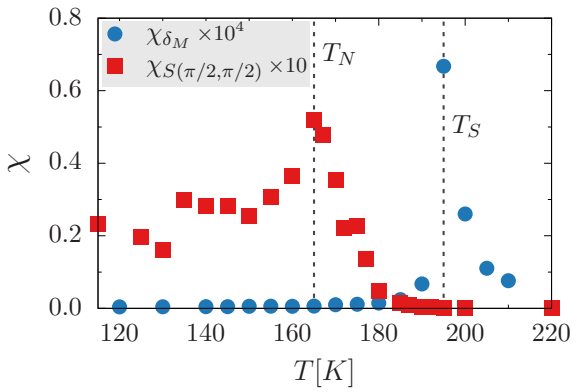

FIG. 4. Magnetic susceptibility χ_S (squares) and monoclinic lattice susceptibility χ_{δ_M} (circles) evaluated using the PTCA algorithm at $\tilde{\lambda}_{12} = 1$ employing a 32×32 sites cluster. In this plot, and other plots of susceptibilities shown below, the fluctuations between subsequent temperatures are more indicative of the error bars than the intrinsic errors bars of individual points, which for this reason are not shown.

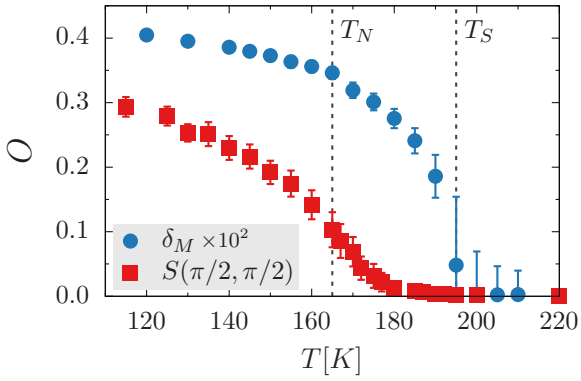

FIG. 5. Magnetic spin structure factor $S(\pi/2,\pi/2)$ (squares) and monoclinic lattice order parameter δ_M (circles) evaluated using the PTCA algorithm for $\tilde{\lambda}_{12} = 1$ on a 32×32 sites cluster.

obtained from the numerical derivative of δ_M as a function of temperature and from monitoring the behavior of the spin-nematic and orbital-nematic order parameters, $\Psi_{NNN}(\mathbf{i})$ and $\Phi_{B_{2g}}(\mathbf{i})$, respectively, introduced in the previous section and their associated susceptibilities.

IV. RESULTS

As explained before, in previous work [23], we found that the magneto-structural transition experimentally observed in FeTe, with $T_S = T_N = 70\,\mathrm{K}$, was reproduced by setting $J_\mathrm{H} = 0.1$ eV and $\tilde{g}_{12} = 0.24$, and by dropping the Heisenberg couplings, i.e., using $J_\mathrm{NN} = J_\mathrm{NNN} = 0$. In the present study for simplicity, we keep fixed the values of all these parameters while we only vary the orbital-lattice coupling $\tilde{\lambda}_{12}$ to investigate whether a nematic phase can be stabilized in a range of temperature. Future work will address what occurs in other portions of parameter space, such as with finite Heisenberg couplings [some partial results are already available (to be shown in future publications) and all indicates that the bicollinear nematic state is still present at large $\tilde{\lambda}_{12}$ even including nonzero J_NN and J_NNN].

A. Special case $\tilde{\lambda}_{12} = 1$

Similarly, as with the behavior reported before for the spin-fermion model in the case of the pnictides with $(\pi,0)$ spin order [27], in the bicollinear case studied here it was also observed that the novel bicollinear nematic region becomes stable by increasing the value of the orbital-lattice coupling. This is not obvious because of competing collinear tendencies, as already explained. Another similarity with the case of the collinear state [27] is that the addition of the orbital-lattice coupling $\tilde{\lambda}_{12}$ turns the first order magnetic transition into a second order one. The temperature width of nematicity remains narrow, as in many previous investigations, and robust values of $\tilde{\lambda}_{12}$ are required. Nevertheless, this is sufficient to demonstrate the matter-of-principle existence of the bicollinear-nematic state discussed in this publication. For clarity, first let us address in detail the largest value of the coupling that we studied which was $\tilde{\lambda}_{12} = 1$.

In Fig. 4, the magnetic susceptibility $\chi_{S(\pi/2,\pi/2)}$ versus temperature is shown. A clear maximum at $T_N = 165\,\mathrm{K}$ indicates the magnetic transition to the bicollinear state with long-range order. The monoclinic lattice susceptibility is also shown. Interestingly, this quantity has a sharp peak at a clearly larger temperature $T_S = 193$ K where the structural transition from tetragonal to monoclinic takes place, indicating that a bicollinear-nematic state does indeed occur.

In Fig. 5, the magnetic structure factor at wave vector $(\pi/2,\pi/2)$ is displayed. The T_N from the susceptibility, shown with a dashed line, should occur when the rate of increase of the order parameter is maximized. This has been verified by performing a spline fit of the $S(\pi/2,\pi/2)$ points obtained from the Monte Carlo simulation and taking the numerical derivative. The monoclinic lattice order parameter δ_M is also presented in Fig. 5. The structural transition temperature is displayed with a dashed line as well. We also verified that the maximum in the lattice susceptibility from Fig. 4 coincides with the maximum rate of change in the lattice order parameter via a spline fit of the Monte Carlo data.

In between the two transition temperatures T_N and T_S, a nematic phase is stabilized. In this phase both short-range orbital and spin-nematic order develop as it can be seen in Fig. 6, where in panel (a), the susceptibilities associated with various order parameters are presented. It can be observed that the orbital-nematic and spin-nematic susceptibilities have maxima at T_S as does the structural susceptibility. This confirms the presence of a monoclinic nematic phase characterized by orbital-nematic and spin-nematic orders. These properties are also reflected in the behavior of the respective order parameters shown in panel (b) of the figure.

Performing spline fits of the order parameters and taking numerical derivatives, the critical temperatures obtained from the susceptibilities were reproduced. It is important to notice that the lattice distortions $\delta_M \sim 10^{-3}$ are quantitatively similar to those reported in FeTe experiments while, as shown in Fig. 6(b), the orbital and spin-nematic order parameters develop values an order of magnitude larger. Thus the strength of the orbital-lattice coupling used still leads to small lattice distortions but appears to generate robust magnetic and orbital

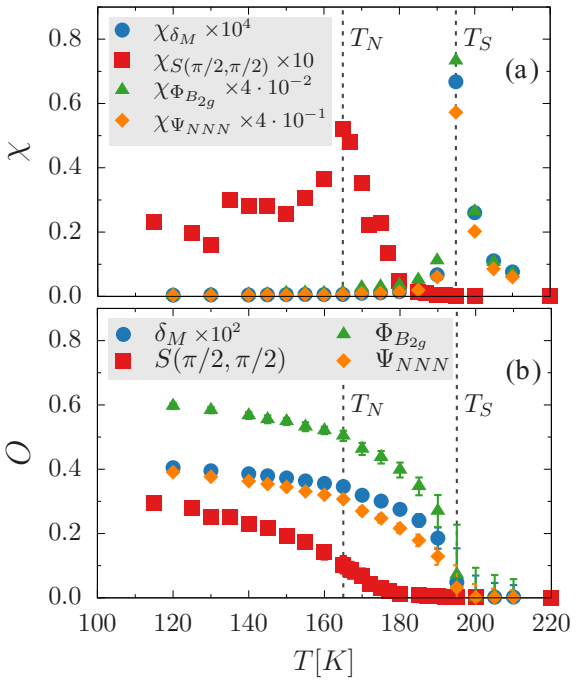

FIG. 6. (a) Magnetic susceptibility $\chi_{S(\pi/2,\pi/2)}$ (red squares) with a maximum at $T_N = 165$ K (dashed line), and the monoclinic lattice susceptibility χ_{δ_M} (blue circles), spin-nematic susceptibility χ_Ψ (orange diamonds), and orbital-nematic susceptibility χ_Φ (green triangles) all with a maximum at $T_S = 193$ K. The susceptibilities were calculated at $\tilde{\lambda}_{12} = 1$ using 32×32 lattices. (b) Monte Carlo measured order parameters associated to (a). Shown are the magnetic structure factor $S(\pi/2,\pi/2)$ (red squares), monoclinic lattice distortion δ_M (blue circles), spin-nematic order parameter Ψ_{NNN} (orange diamonds), and orbital-nematic order parameter $\Phi_{B_{2g}}$ (green triangles). The transition temperatures were obtained from the susceptibilities in (a) and via numerical derivatives in (b). Both procedures give the same result.

short-range order inducing substantial anisotropic effects in these observables.

B. Special case $\tilde{\lambda}_{12} = 0.85$

As the value of the orbital-lattice coupling is reduced the separation between the magnetic and the structural transitions decreases. In panel (a) of Fig. 7, the magnetic and structural susceptibilities at $\tilde{\lambda}_{12} = 0.85$ obtained from Monte Carlo simulations are presented. In this case $T_N = 145$ K, while $T_S = 147$ K. The orbital- and spin-nematic order parameters also have a maximum susceptibility at T_S (not shown for simplicity). The magnetic and structural order parameters are shown in panel (b) of Fig. 7 and their qualitative behavior is in agreement with panel (a). The indicated transition temperatures have been obtained from numerical fits of the order parameters and their derivatives as described in the previous subsection. This case $\tilde{\lambda}_{12} = 0.85$ is close to the limit of our numerical accuracy. In principle, it is possible that simulations using larger systems and with far more statistics may unveil a very narrow bicollinear nematic state even for small values of $\tilde{\lambda}_{12}$. However, for our qualitative purposes, simply showing the stability of the new proposed phase in any range of $\tilde{\lambda}_{12}$ is sufficient.

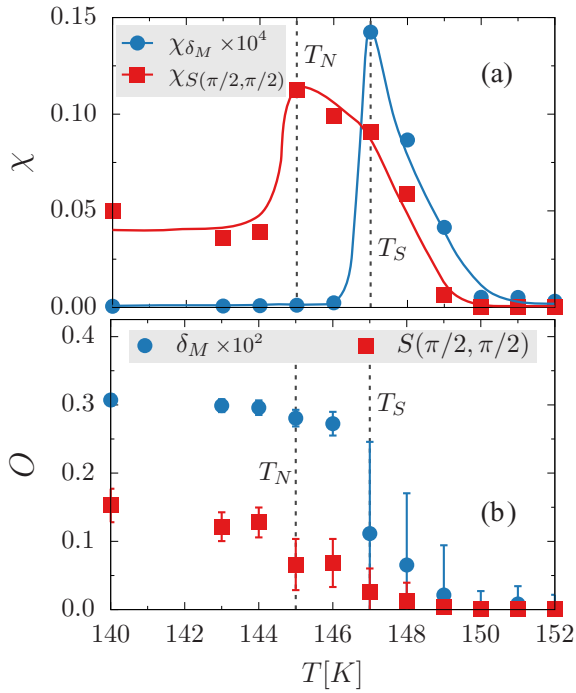

FIG. 7. (a) Susceptibilities associated with the magnetic spin structure factor $S(\pi/2,\pi/2)$ (squares) and with the monoclinic lattice distortion (circles) using $\tilde{\lambda}_{12} = 0.85$ and a 32×32 cluster. Solid lines are guides to the eye. (b) Spin structure factor $S(\pi/2,\pi/2)$ (squares) and monoclinic lattice order parameter δ_M (circles) for the same $\tilde{\lambda}_{12}$ and cluster size as in (a).

C. Phase diagram

The phase diagram obtained as a function of the orbital-lattice coupling $\tilde{\lambda}_{12}$ and temperature is presented in Fig. 8. It can be seen that the region with B_{2g} nematicity can be stabilized at robust values of the orbital-lattice coupling. While a very narrow nematic phase may exist at smaller values of this coupling, numerically we have been able to

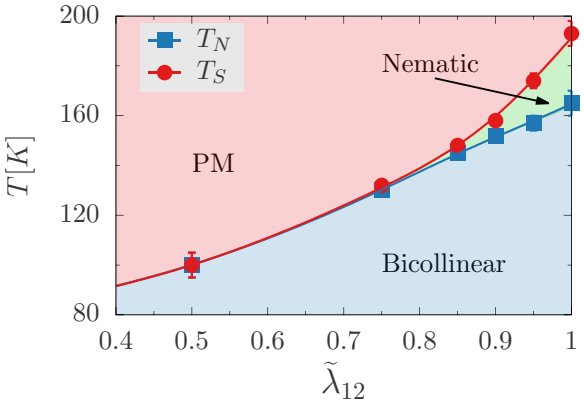

FIG. 8. Phase diagram varying temperature and $\tilde{\lambda}_{12}$, for $\tilde{g}_{12} = 0.24$, $J_H = 0.1$ eV, and $J_{NN} = J_{NNN} = 0.0$. Note the narrow temperature width of stability of the bicollinear-nematic state, similarly as it occurs for the more standard $(\pi,0) - (0,\pi)$ nematic state [27]. For values of $\tilde{\lambda}_{12}$ smaller than 0.75, our numerical accuracy does not allow us to distinguish between T_N and T_S.

resolve the separation between the two critical temperatures only for $\tilde{\lambda}_{12} \geqslant 0.75$. As described in the previous sections, the separation between T_N and T_S monotonically increases with $\tilde{\lambda}_{12}$.

V. DISCUSSION AND POSSIBLE PHYSICAL REALIZATIONS

Our results have illustrated the possible existence of a nematic phase involving bicollinear short-range order, using as explicit example a computational study of the spin-fermion model incorporating the lattice distortions corresponding to the iron telluride family. Previous investigations [23] showed that the addition to the electronic spin-fermion model for pnictides of a coupling between a spin-nematic order parameter with B_{2g} symmetry and the monoclinic distortions of the iron lattice does induce the low-temperature monoclinic and spin bicollinear state experimentally observed in FeTe. That result was remarkable because the spin-fermion model contains a tight-binding term that favors the $(\pi,0)$ and $(0,\pi)$ collinear states that arise from the nesting of the Fermi surface in weak coupling. However, the $\tilde{g}_{12}$ spin-lattice interaction, when sufficiently strong, can overcome these tendencies and stabilize the monoclinic bicollinear state.

Here, we have included an additional orbital-lattice term with coupling strength $\tilde{\lambda}_{12}$, involving the monoclinic lattice strain coupled to an orbital order parameter with B_{2g} symmetry. By this procedure, we have shown that a novel nematic phase characterized by the breakdown of the lattice rotational symmetry between the two possible diagonal directions of the spin bicollinear state can be induced. In this new nematic phase, short-range spin- and orbital-nematic order develop accompanied by a lattice monoclinic distortion.

The model Hamiltonian studied here only allows us to show explicitly, as a matter of principle, that indeed the bicollinear-nematic state described above does occur in computational studies once all of the many degrees of freedom and couplings are properly incorporated. But it is difficult to predict on what specific material this subtle state will be realized in practice, thus we can only discuss some scenarios qualitatively. The possible splitting of T_N and T_S by electron doping was raised in [9]. However, spin-fermion model studies including doping but not quenched disorder (i.e., in the "clean" limit) did not detect such a split, at least in the doping range studied (Fig. 2 of Ref. [28]). Another generic qualitative observation is that in the pnictides nematicity is observed for the 1111 compounds even in the undoped limit [11]. Thus, to find the B_{2g} nematic phase discussed here, it may be necessary to synthesize materials with intercalated FeTe planes.

However, in our opinion, the most likely scenario to stabilize the proposed bicollinear-nematic regime in variations of the FeTe compound is by the chemical replacement of iron by other transition metal elements, thus simultaneously modifying the electronic density as well as the amount of quenched disorder. In pnictides, replacing Fe by Co, Ni, or Cu indeed leads to a wide nematic region. Our previous computational investigations using the spin-fermion model with doping and disorder [28] clearly showed that indeed by this procedure a $(\pi,0)$ nematic temperature range can be induced even in cases where T_N and T_S coincide in a first-order transition for the undoped parent compound, as in the 122 family. Disorder plays a more important role than doping in this split [28], as observed experimentally as well [40]. To our knowledge, the experimental investigations of (Fe,X)Te, with X another transition metal element, are very limited. We are aware of three main lines of investigations and conclusions:

(i) Copper doping of FeTe was studied in Refs. [41,42] for two Cu concentrations using single crystals. For the case $Fe_{1.06}Cu_{0.04}Te$, the presence of strain was detected at 41 K upon cooling [41]. At lower temperatures, approximately 36 K, nearly commensurate long-range bicollinear magnetic order occurs. The presence of two transitions seems in agreement with our prediction of bicollinear nematicity. However, in Ref. [41], it was argued that between 36 and 41 K, the lattice distortion could be orthorhombic as in pnictides. The possible competition with orthorhombic tendencies was theoretically addressed and reported in Ref. [23]. This competition adds an extra complication to the detection of the here predicted bicollinear-nematic state. For the case $FeCu_{0.1}Te$, only cluster glass behavior was found below 22 K, presumably due to disorder [41]. Note that this glassy state could be nematic.

(ii) The case of Ni doping was reported for the compounds $Fe_{1.1-x}Ni_xTe$ with $x = 0,0.02,0.04,0.08$, and 0.12 [43]. Magnetization studies show that T_N decreases with increasing x up to 0.04, while for $x = 0.08,0.12$ a possible spin glass transition was reported. In fact, neutron diffraction at $x = 0.12$ found neither structural nor magnetic transitions at low temperatures. Since this study focused on long-range magnetic order, the presence of bicollinear nematicity is still possible.

(iii) Cobalt doping has also been recently studied via single crystals of $Fe_{1+y-x}Co_xTe$ with $x = 0,0.01,0.04,0.07,0.09$, and 0.11 [44]. In the range up to $x = 0.07$, the antiferromagnetic transition systematically decreases. For $x = 0.09$ and larger, the long-range-order transition disappears.

As a partial summary, the available experimental literature on (Fe,X)Te does not conclusively show neither the presence nor absence of bicollinear-nematicity, and more work is needed to clarify this matter now in the light of our present study. For example, in the context of pnictides the pioneering studies of $Ba(Fe_{1-x}Co_x)_2As_2$ [7] reported the resistivities vs. temperature along the a and b axes, highlighting their different behavior and substantial differences particularly below $x = 0.07$. Similar careful studies in the (Fe,X)Te context must be performed but focusing on the temperature evolution of the resistivities along and perpendicular to the main spin diagonals in the bicollinear state, as already performed for FeTe [45,46]. In addition, recent inelastic neutron scattering studies of nematicity in $BaFe_{1.935}Ni_{0.065}As_2$ [47] focused on the temperature dependence of the intensity of the peaks at $(\pi,0)$ and $(0,\pi)$, reporting their split at T_S with cooling, followed by a collapse to zero of the $(0,\pi)$ intensity at T_N. Similar studies for X-doped FeTe (X = Cu,Ni,Co) should be carried for the temperature dependence of the neutron intensities corresponding to the $(\pi/2,\pi/2)$ and $(\pi/2,-\pi/2)$ wave vectors.

We also would like to point out that our work confirms that magnetoelastic effects tend to estabilize the bicollinear state, while in the absence of this kind of coupling Q plaquette or orthogonal double stripe order could be stabilized, which may be the case in FeTe with excess iron [48,49]. In addition, in a

recent publication [50] a double-stage nematic bond-ordering above the bicollinear state was proposed, but this effect would be difficult to study numerically due to the narrow range of the nematic phase.

VI. CONCLUSIONS

In this publication, based on simple symmetry observations and a concrete model Hamiltonian numerical simulation, we have argued that the exotic bicollinear state known to be stable in FeTe admits a possible nematic state above the antiferromagnetic critical temperature. In other words, as discussed in the previous section, via chemical substitution it is conceivable that a split of the first-order transition of FeTe could be generated. Upon cooling, this would induce first a T_S, where the B_{2g} monoclinic distortion is stabilized and short-range spin and orbital order develops breaking the lattice rotational invariance, and second a T_N at a lower temperature, where long-range bicollinear order is fully stabilized. Experimentally finding this new exotic state not only would confirm the theoretical prediction outlined here, but it would allow us to investigate to what extend nematic fluctuations are needed to induce superconductivity.

ACKNOWLEDGMENTS

C.B.B. was supported by the National Science Foundation, under Grant No. DMR-1404375. E.D., J.H., and A.M. were supported by the US Department of Energy, Office of Basic Energy Sciences, Materials Sciences and Engineering Division.

[1] D. C. Johnston, Adv. Phys. **59**, 803 (2010).
[2] P. J. Hirschfeld, M. M. Korshunov, and I. I. Mazin, Rep. Prog. Phys. **74**, 124508 (2011).
[3] Z. P. Yin, K. Haule, and G. Kotliar, Nat. Mater. **10**, 932 (2011).
[4] P. C. Dai, J. P. Hu, and E. Dagotto, Nat. Phys. **8**, 709 (2012).
[5] E. Dagotto, Rev. Mod. Phys. **85**, 849 (2013).
[6] R. M. Fernandes, A. V. Chubukov, and J. Schmalian, Nat. Phys. **10**, 97 (2014).
[7] J.-H. Chu, J. G. Analytis, K. De Greve, P. L. McMahon, Z. Islam, Y. Yamamoto, and I. R. Fisher, Science **329**, 824 (2010).
[8] I. R. Fisher, L. Degiorgi, and Z. X. Shen, Rep. Prog. Phys. **74**, 124506 (2011).
[9] R. M. Fernandes, A. V. Chubukov, J. Knolle, I. Eremin, and J. Schmalian, Phys. Rev. B **85**, 024534 (2012).
[10] R. M. Fernandes and J. Schmalian, Supercond. Sci. Technol. **25**, 084005 (2012).
[11] C. de la Cruz, Q. Huang, J. W. Lynn, J. Li, W. Ratcliff II, J. L. Zarestky, H. A. Mook, G. F. Chen, J. L. Luo, N. L. Wang, and P. Dai, Nature (London) **453**, 899 (2008).
[12] C. R. Rotundu and R. J. Birgeneau, Phys. Rev. B **84**, 092501 (2011).
[13] S. Kasahara, H. J. Shi, K. Hashimoto, S. Tonegawa, Y. Mizukami, T. Shibauchi, K. Sugimoto, T. Fukuda, T. Terashima, A. H. Nevidomskyy, and Y. Matsuda, Nature (London) **486**, 382 (2012).
[14] R. Zhou, Z. Li, J. Yang, D. L. Sun, C. T. Lin, and G.-q. Zheng, Nat. Commun. **4**, 2265 (2013).
[15] Q. Huang, Y. Qiu, Wei Bao, M. A. Green, J. W. Lynn, Y. C. Gasparovic, T. Wu, G. Wu, and X. H. Chen, Phys. Rev. Lett. **101**, 257003 (2008).
[16] X. Chen, P. Dai, D. Feng, T. Xiang, and F.-C. Zhang, Natl. Sci. Rev. **1**, 371 (2014).
[17] S. R. Saha, N. P. Butch, T. Drye, J. Magill, S. Ziemak, K. Kirshenbaum, P. Y. Zavalij, J. W. Lynn, and J. Paglione, Phys. Rev. B **85**, 024525 (2012).
[18] W. Bao, Y. Qiu, Q. Huang, M. A. Green, P. Zajdel, M. R. Fitzsimmons, M. Zhernenkov, S. Chang, M. Fang, B. Qian, E. K. Vehstedt, J. Yang, H. M. Pham, L. Spinu, and Z. Q. Mao, Phys. Rev. Lett. **102**, 247001 (2009).
[19] S. Li, C. de la Cruz, Q. Huang, Y. Chen, J. W. Lynn, J. Hu, Y. L. Huang, F. C. Hsu, K. W. Yeh, M. K. Wu, and P. Dai, Phys. Rev. B **79**, 054503 (2009).
[20] The bicollinear state is also known as the E-phase in manganites: T. Hotta, M. Moraghebi, A. Feiguin, A. Moreo, S. Yunoki, and E. Dagotto, Phys. Rev. Lett. **90**, 247203 (2003); See also E. Dagotto, T. Hotta, and A. Moreo, Phys. Rep. **344**, 1 (2001).
[21] G. F. Chen, Z. G. Chen, J. Dong, W. Z. Hu, G. Li, X. D. Zhang, P. Zheng, J. L. Luo, and N. L. Wang, Phys. Rev. B **79**, 140509(R) (2009).
[22] D. Fobes, I. A. Zaliznyak, Z. Xu, R. Zhong, G. Gu, J. M. Tranquada, L. Harriger, D. Singh, V. O. Garlea, M. Lumsden, and B. Winn, Phys. Rev. Lett. **112**, 187202 (2014); In this reference, an electronic delocalization transition was proposed to lift the $xz = yz$ orbital degeneracy, leading to ferro-orbital order along the ferromagnetic zigzag chains of the bicollinear state of $Fe_{1+y}Te$; See also I. Zaliznyak, A. T. Savici, M. Lumsden, A. Tsvelik, R. Hu, and C. Petrovic, Proc. Natl. Acad. Sci. USA **112**, 10316 (2015).
[23] C. B. Bishop, A. Moreo, and E. Dagotto, Phys. Rev. Lett. **117**, 117201 (2016).
[24] There are alternative explanations for the iron telluride state: (1) recent results indicate charge ordering in FeTe. See W. Li, W.-G. Yin, L. Wang, K. He, X. Ma, Q.-K. Xue, and X. Chen, Phys. Rev. B **93**, 041101(R) (2016); (2) a spin 1 model with ring-exchange interactions can also explain the bicollinear state. See H.-H. Lai, S.-S. Gong, W.-J. Hu, and Q. Si, arXiv:1608.08206.
[25] P. Chandra, P. Coleman, and A. I. Larkin, Phys. Rev. Lett. **64**, 88 (1990).
[26] Notice that the magnetic structure factor for the state in Fig. 1(a) [Fig. 1(b)] has peaks at both momentum $(\pi/2, -\pi/2)$ and $(-\pi/2,\pi/2)$ $[(\pi/2,\pi/2)$ and $(-\pi/2, -\pi/2)]$.
[27] S. Liang, A. Moreo, and E. Dagotto, Phys. Rev. Lett. **111**, 047004 (2013).
[28] S. Liang, C. B. Bishop, A. Moreo, and E. Dagotto, Phys. Rev. B **92**, 104512 (2015).

[29] M. Hoyer, R. M. Fernandes, A. Levchenko, and J. Schmalian, Phys. Rev. B **93**, 144414 (2016).
[30] W.-G. Yin, C.-C. Lee, and W. Ku, Phys. Rev. Lett. **105**, 107004 (2010).
[31] S. Liang, G. Alvarez, C. Sen, A. Moreo, and E. Dagotto, Phys. Rev. Lett. **109**, 047001 (2012).
[32] The presence of both itinerant and localized characteristics in neutron experiments for $Fe_{1.1}Te$ suggests the spin-fermion model is reasonable for iron tellurides. See I. A. Zaliznyak, Z. Xu, J. M. Tranquada, G. Gu, A. M. Tsvelik, and M. B. Stone, Phys. Rev. Lett. **107**, 216403 (2011).
[33] S. Liang, A. Mukherjee, N. D. Patel, C. B. Bishop, E. Dagotto, and A. Moreo, Phys. Rev. B **90**, 184507 (2014).
[34] M. Daghofer, A. Nicholson, A. Moreo, and E. Dagotto, Phys. Rev. B **81**, 014511 (2010).
[35] The magnitude of the localized spins is set to $S_i = 1$ since its actual value can be absorbed into the Hamiltonian parameters.
[36] Some calculations (not shown) for various sets of Heisenberg couplings, keeping $J_{NNN}/J_{NN} = 2/3$ constant, were performed for selected values of $\tilde{\lambda}_{12}$ and $\tilde{g}_{12}$. Only quantitative changes in the presented results were observed, while qualitatively they were similar. Thus the inclusion of Heisenberg couplings, which favor collinear order, does not destabilize the fragile bicollinear nematic state, at least in the regime of robust lattice-orbital coupling. Details will be presented in future publications.
[37] H.-H. Kuo, J.-H. Chu, S. A. Kivelson, and I. R. Fisher, Science **352**, 958 (2016).
[38] A. Mukherjee, N. D. Patel, C. B. Bishop, and E. Dagotto, Phys. Rev. E **91**, 063303 (2015).
[39] S. Kumar and P. Majumdar, Eur. Phys. J. B **50**, 571 (2006).
[40] N. Ni, A. Thaler, J. Q. Yan, A. Kracher, E. Colombier, S. L. Bud'ko, P. C. Canfield, and S. T. Hannahs, Phys. Rev. B **82**, 024519 (2010).
[41] J. Wen, Z. Xu, G. Xu, M. D. Lumsden, P. N. Valdivia, E. Bourret-Courchesne, G. Gu, D.-H. Lee, J. M. Tranquada, and R. J. Birgeneau, Phys. Rev. B **86**, 024401 (2012).
[42] P. N. Valdivia, M. G. Kim, T. R. Forrest, Z. Xu, M. Wang, H. Wu, L. W. Harringer, E. D. Bourret-Courchesne, and R. J. Birgeneau, Phys. Rev. B **91**, 224424 (2015), and references therein.
[43] J. Janaki, T. G. Kumary, N. Thirumurugan, A. Mani, A. Das, G. V. N. Rao, and A. Bharathi, J. Supercond. Nov. Magn. **25**, 209 (2012).
[44] Y. Zhu, L. Li, Z. Yang, Z. Zhang, B. Yuan, J. Chen, H. Du, Y. Sun, and Y. Zhang, J. Magn. Magn. Mater. **397**, 1 (2016).
[45] L. Liu, T. Mikami, M. Takahashi, S. Ishida, T. Kakeshita, K. Okazaki, A. Fujimori, and S. Uchida, Phys. Rev. B **91**, 134502 (2015).
[46] J. Jiang, C. He, Y. Zhang, M. Xu, Q. Q. Ge, Z. R. Ye, F. Chen, B. P. Xie, and D. L. Feng, Phys. Rev. B **88**, 115130 (2013).
[47] W. Zhang, J. T. Park, X. Lu, Y. Wei, X. Ma, L. Hao, P. Dai, Z. Y. Meng, Y.-f. Yang, H. Luo, and S. Li, Phys. Rev. Lett. **117**, 227003 (2016).
[48] S. Ducatman, N. B. Perkins, and A. Chubukov, Phys. Rev. Lett. **109**, 157206 (2012).
[49] S. Ducatman, R. M. Fernandes, and N. B. Perkins, Phys. Rev. B **90**, 165123 (2014).
[50] G. Zhang, J. K. Glasbrenner, R. Flint, I. I. Mazin, and R. M. Fernandes, Phys. Rev. B **95**, 174402 (2017).